35th Annual International Conference of the IEEE EMBS
Osaka, Japan, 3 - 7 July, 2013

# A 24 $V_{pp}$ Compliant Biphasic Stimulator for Inductively Powered Animal Behavior Studies

Sudip Nag[1], Dinesh Sharma[2] and Nitish V. Thakor[3]

***Abstract*— Stimulation of biological neurons using electrical charges has gained popularity in neuro-engineering studies. Wireless power delivery to electrical stimulators is an essential requirement for long term and maintenance-free implantable applications. Voltage compliance is often a limiting factor in these systems. We present an inductively powered biphasic stimulator that is capable of exhibiting 24 $V_{pp}$ load voltage compliance, while harvesting up to 13 V. The stimulator can deliver currents ranging from 10 $\mu$A to 6 mA. The inductive energy harvesting system operates at a low carrier frequency of 134.2 KHz for enhanced depth of penetration in biological medium. The near-field harvester works reliably for up to 50 mm inter-antenna distance. Noise performance and charge balancing accuracy have also been improved due to the absence of a boost switching circuit and floating current source based architecture. *In-vivo* motor and visual cortex stimulations have been performed using epi-dural screw electrodes on an awake behaving and anesthetized Wister rat.**

## I. Introduction

Electrical stimulation using biphasic current pulses is a well-known technique to evoke responses in neuronal systems. Functional electrical stimulations and prosthetic applications can greatly benefit from such a technique. Wireless power delivery to electrical stimulators is very important to reduce maintenance in implantable operation. However, inadequate output voltage compliance is a limiting factor. This results from losses in inductive energy transmission through biological medium [1], voltage drop in stimulators and high impedance of interface microelectrodes. Low voltage compliance may lead to insufficient stimulus current and distorted pulses, which in turn, adversely affects charge balancing and biological safety [2].

Commonly used mega-Hertz power carriers [3]–[5] can adversely affect range of inductive power delivery due to skin-effect [1], and also reduces voltage compliance. Forcing 200 $\mu$A through a 100 K$\Omega$ electrode would require 20 V compliance at the output of the stimulator. Enhanced voltage compliance is realizable through separate rectifiers and filters for positive and negative supplies [5], [6] or by using switch-mode voltage boosters [7]. Size of stimulator, dynamic power loss and switching noise increase in these approaches.

[1]Sudip Nag is with the Singapore Institute for Neurotechnology (SINAPSE), National University of Singapore, Singapore. sudipnag1@nus.edu.sg

[2]Dinesh Sharma is with the Department of Electrical Engineering, Indian Institute of Technology, Bombay, India. dinesh@ee.iitb.ac.in

[3]Nitish V. Thakor is with the Department of Biomedical Engineering, Johns Hopkins University, USA, and, the Singapore Institute for Neurotechnology (SINAPSE), National University of Singapore, Singapore. nitish@jhu.edu, sinapsedirector@gmail.com

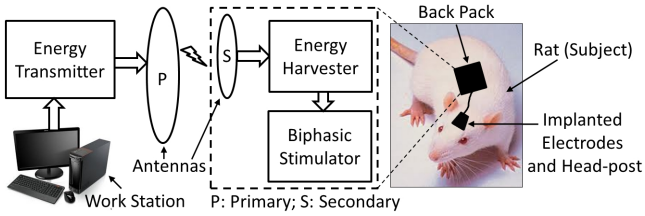


Fig. 1. Block diagram of the wirelessly powered high voltage stimulator.

We present a high voltage stimulator that is capable to generate up to 24 $V_{pp}$ load compliance while harvesting energy through an inductively coupled 134.2 KHz wireless link. Harvested DC voltage ranges up to 13 V, while the coil separation works up to 50 mm. The architecture utilizes harvested supply in bipolar fashion to deliver peak-peak load voltage compliance up to 24 V. Charge balancing has been realized by means of a biphasic constant current stimulator, which is capable of forcing up to 6 mA. Floating current sources and steering diodes are used in the analog front-end of the stimulator. Validations and animal trials have been performed on an awake behaving and anesthetized rodent model (Wister rat).

The rest of this paper is organized as follows: Section II states system architecture and design considerations. Sections III and IV present measurement results with electrical performance and animal studies. Section V summarizes the paper with prospective future applications.

## II. System Architecture

The block-diagram of the wirelessly powered stimulator has been depicted in Fig. 1. The primary side consists of an energy transmitter and an antenna (coil). The energy transmitter consists of an oscillator and a power driver stage. The computer work station sends commands for *ON-OFF* and system controls. The secondary side antenna (coil) and the energy harvester receive energy through transformer-like action. The energy harvester and the stimulator blocks are mounted as a back-pack on the subject. Harvested energy has been utilized by the biphasic stimulator to produce large voltage compliant and charge balanced current pulses through implanted electrodes over the brain regions in the animal subject.

### A. Principles of Operation

The neuro-stimulator architecture adopts three main principles of operation. Firstly, low frequency inductive coupling has been utilized for longer depth of penetration in biological

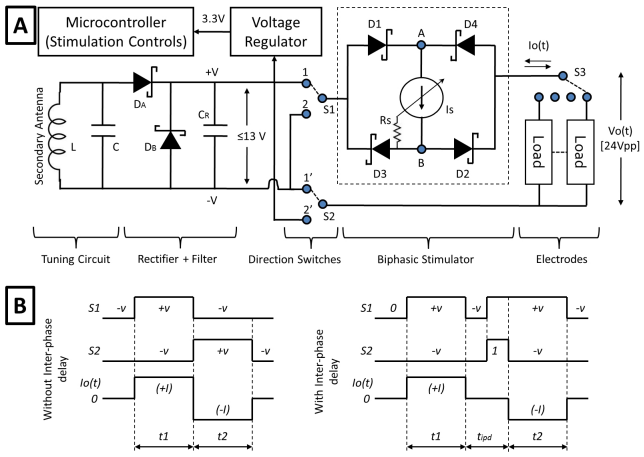


Fig. 2. Schematic and timing diagrams of the large voltage compliant wireless stimulator.

media (eg. tissues). Secondly, harvested single supply DC voltage has been utilized separately for positive and negative phases of biphasic stimulation. Thirdly, a floating current source and identical phase duration based constant current stimulator has been important for accurate charge balance and biological safety. Enhanced output voltage compliance and reliable operation are realizable by means of combining the above principles.

### B. Architecture and Operation

Fig. 2 depicts the schematic of the large voltage compliance charge balanced stimulator (secondary side). The energy harvesting front-end consists of a parallel LC tuned power receiving coil, a low drop-out rectifier and filter, a unidirectional constant current source, a full bridge steering or conveyor network, and an output demultiplexer. A low speed microcontroller (e.g. 4 KHz) generates switch controls and timing signals through its *IO* (input-output) pins, while reducing dynamic power consumption. A low quiescent current low drop-out voltage regulator has been used to provide 3.3 V to the microcontroller. The switches, $S1$ and $S2$, control the direction of stimulation currents. The switch $S3$ is a demultiplexer that selects electrode channels. All the switches are low on-resistance type for reduced voltage drop.

Magnitude of the output current is adjustable through hardware configuration of the current control resistor $R_s$. Voltages at pole terminals of $S1$ and $S2$ determine the direction of output current. Positive load currents are conveyed through the nodes $S1$, $A$, $B$, $S3$ and $S2$, while diode $D1$ and $D2$ are forward biased. Negative load currents take the path through the nodes $S2$, $S3$, $A$, $B$ and $S1$, while $D3$ and $D4$ are forward biased. It is important to note that irrespective of the directions of load current, the constant current source conducts uni-directionally.

A floating constant current source is an important choice for better charge balancing and $zero$ quiescent current operation. This is operated through shunt drop-out voltage of $\geq$ 1 V [8]. A schottky diode based current steering network ensures fast *ON/OFF* transitions and low *ON* state voltage drops. Faster switching improves speed or dynamic performance, whereas, low on-state drop is beneficial for increased voltage compliance. Steering action relies on relative voltages at $S1$ and $S2$. Additional switch controls and feed-through noise have been avoided by linear-mode operation to ensure precise charge balancing.

### C. Design Considerations

*1) Voltage Compliance Enhancement:* Voltage compliance is enhanced through better antenna coupling, enhanced range of power delivery and low-drop bipolar operation of the stimulator front-end. In addition, the stimulator adopts the strategy to utilize available rail-rail DC harvested voltage for both positive and negative stimulation cycles, separately. This is important to realize the compliance close to two-times than the supply voltage.

The stimulator drives the node $S1$ to $+V$ and S2 to $-V$ during positive and vice-versa during negative stimulation phases, respectively. Theoretically, the stimulator offers a maximum load voltage of $2(|V_{dd} - V_{drop}|)$. Considering, $Vdd = +V - (-V) = 13V$ and $V_{drop}$ is 1 V, the peak-peak load voltage range is 24 V.

*2) Inter-phase Delays:* Inter-phase delays (IPD) may be added between positive and negative stimulation phases by means of controlling voltage difference between the control nodes $S1$ and $S2$. The switches $S1$ and $S2$ must be either configured at equal voltage level ($+V$ or $-V$) or floating during inter-phase delays.

*3) Stimulation Speed:* Maximum frequency of stimulation depends upon output capacitance of the stimulator and dynamics of the control signals. The microcontroller can control up to 2 KHz biphasic signals. However, upper limit of stimulation frequency is limited by the rise and fall times of output voltage. The analog front-end of the stimulator can operate up to 30 KHz.

## III. Electrical Measurements

The stimulator hardware has been realized using commercially available components for proof-of-concept and rapid prototyping. Measured electrical characteristics are described below.

### A. Stimulation Waveforms

Measured load voltage and current waveforms are shown in Fig. 3 while passing anodic-first 100 $\mu$A biphasic currents (top trace) through a 100 K$\Omega$ resistor load and with 10 mm antenna separation. Differentially measured output voltage across the load is 20 $V_{pp}$ (middle trace). However, absolute voltage across the same load never exceeds 12 V (bottom trace), which is close to the harvested DC value.

### B. Voltage Compliance

Peak-peak load voltage compliance of the stimulator has been stated in Fig. 4 as a function of the harvested DC voltage. The *y-axes* show peak-peak load voltage compliance (left) and relative percentage (right) with respect to actual

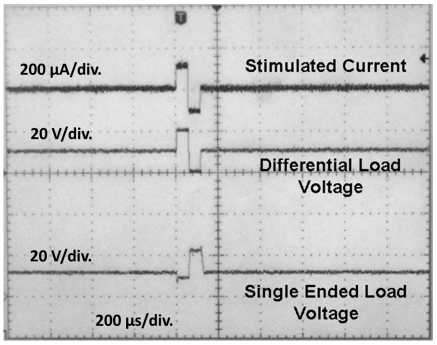


Fig. 3. Oscilloscope screenshot showing electrode or stimulated current, differential voltage across the load and absolute or single-ended load voltage across a resistor load.

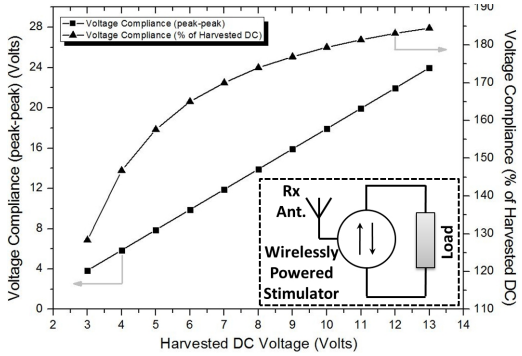


Fig. 4. Output (electrode) voltage compliance as a function of harvested voltage in the secondary side of the inductively powered stimulator.

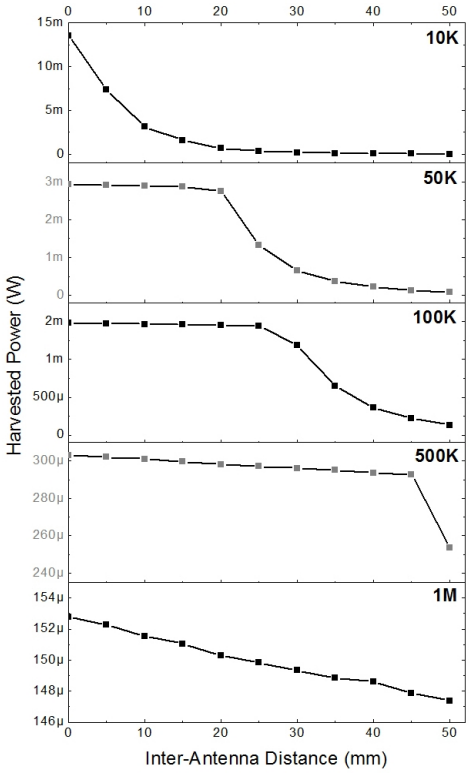


Fig. 5. Harvested power as functions of inter-antenna distances and load impedance.

harvested voltage (*x-axis*). Peak-peak output voltage compliance has always been found to be larger than the harvested DC power supply.

### C. Harvested Power

Harvested power has been measured using load impedances at varied inter-antenna separation, while the transmitter side was operated at 15 V. Fig. 5 shows relations between harvested power dissipation and inter-antenna distance. Low impedance loads can dissipate more power for the given inter-antenna separation, as compared to larger impedance loads, and vice-versa.

### D. Current and Charge Accuracy

Charge balancing accuracy has been very high, mainly due to biphasic current matching using a floating current source based architecture. Current error has been less than 27 pA for 1.4 mA stimulation. Charge error (per cycle) is found less than 5.6 fC for 140 nC injections. The results have been obtained using a resistor-capacitor series circuit and post-stimulation baseline voltage analysis [9].

### E. Power Consumption

The low frequency (4 KHz) operated microcontroller (MSP430F2274, Texas Instruments) based timing generator consumes approximately 1.6 $\mu$W at 3.3V supply while controlling 100 Hz stimulations. *Zero* quiescent power is additionally consumed by the stimulator front-end [9]. Table I lists the measured electrical specifications and comparison with other high voltage stimulators.

TABLE I
SPECIFICATIONS AND COMPARISON WITH OTHER HIGH VOLTAGE STIMULATORS

| Parameters | This work | [7] | [5] |
|---|---|---|---|
| Voltage Compliance | Up to 24 $V_{pp}$ | 20 V | 20 V |
| Harvested Voltage | Up to 13 V | 11.1 V | 10 V |
| Harvested Power | 3 mW at 1 cm | NA | NA |
| Carrier Frequency | 134.2 KHz | 13.56 MHz | 13.56 MHz |
| Charge Balance | 5.6 fC | NA | 15 % |
| Stimulator Mode | Bipolar | NA | Monopolar |

NA: Not Available

## IV. In-Vivo Measurements

### A. Experimental Arrangement

Animal trials have been performed with cortical stimulations in Wister rat, as per the Johns Hopkins University Animal Care and Use Committee approval. Chronic implantation of epidural stainless-steel electrodes have been made over the motor ($M1$ region) and visual ($V1$) cortex regions in a female subject (340 g), as shown in Fig. 6. The reference electrode was located right-anterior to bregma. Silicone insulated electrode connection wires were taken to a biocompatible (teflon) connector, which was affixed with

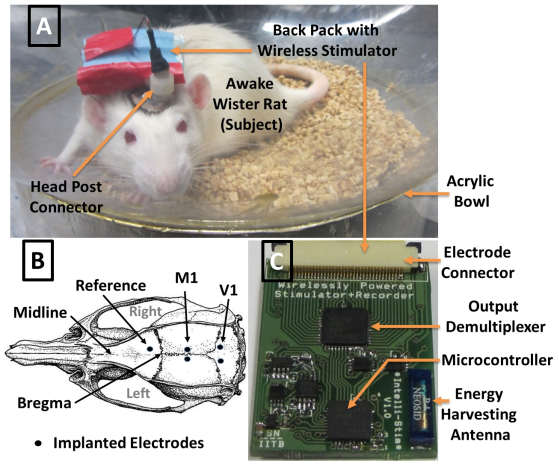


Fig. 6. A. Awake behaving rat with the back-pack stimulator and the implanted electrodes; B. Stain-less steel electrode locations over cortical regions; C. Printed circuit board for the large voltage complaint stimulator.

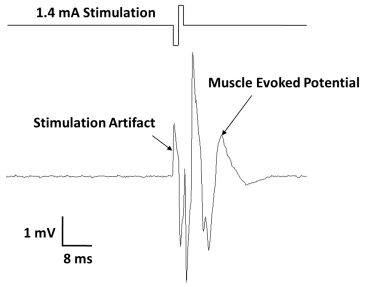


Fig. 7. Muscle Evoked Potentials (MEPs) from the forelimb in anesthetized condition.

dental cement over the skull. Thereafter, the animal was allowed to recover for two weeks.

The wirelessly powered stimulator hardware was mounted as a back-pack on the rat during experiments. Electrode connection was established through a mating connector. Awake-behaving experiments were performed with the subject freely released in an 18-inch transparent acrylic bowl. Thereafter, anesthetized recording of muscle evoked potentials (MEPs) caused by $M1$ stimulation were recorded at the forelimbs. A commercially available 3-wire amplifier system (TDT RA16PA preamplifier and RX5 base station) was connected through an optical isolator. The energy radiating antenna was kept in proximity to the back-pack in all the cases.

### B. Stimulation and Recording

Non-overlapped stimulation pulses up to 6 mA (peak) were applied to the $M1$ and $V1$ regions. The left and the right hemispheres were activated sequentially. Physical movement and MEP signals were observed from the forelimbs, in case of $M1$ stimulations (Fig. 7). However, $V1$ stimulation revealed eye-blinks in awake condition, probably due to sensation of phosphenes.

Anodic-first and cathodic-first stimulation pulses were applied during all trials. Cathodic-first pulses caused more observable effects than anodic-first ones, which is probably due to better depolarization effect of neurons in the cortex.

## V. Conclusions

A wirelessly powered stimulator with large voltage compliance has been presented in this paper. Output voltage compliance of the stimulator ranges up to 24 $V_{pp}$, while harvesting 13 V from an inductively powered source. A low frequency (134.2 KHz) power carrier has been used for enhanced depth of penetration up to 50 mm. The system can harvest more than 3 mW power for 10 mm antenna separation and 10 KΩ load. The floating current source and the steering network based charge balanced stimulator exhibits better than 5.6 fC accuracy for 140 nC stimulations. The stimulator can generate anodic-first or cathodic-first stimulation pulses up to 6 mA, and optional inter-phase delay. The power requirement is quite low due to the simple architecture and small dynamic losses.

The stimulator has been tested in an *in-vivo* rodent model under awake-behaving and anesthetized conditions. The system is suitable for application with high impedance microelectrodes as found in high density implants. Future goals include further miniaturization and increase in energy transfer efficiency.

## Acknowledgment

The authors would like to thank Tata Consultancy Services for graduate student fellowship and Dr. Yama Akbari for chronic implantation of electrodes.

## References

[1] S. Mandal, L. Turicchia, and R. Sarpeshkar, "A low-power, battery-free tag for body sensor networks," *IEEE Pervasive Computing*, vol. 9, no. 1, pp. 71–77, Mar. 2010.

[2] J. C. Lilly, J. R. Hughes, E. C. Alvord-Jr., and T. W. Galkin, "Brief, noninjurious electric waveform for stimulation of the brain," *Science*, vol. 121, no. 3144, pp. 468–469, Apr. 1955.

[3] S. K. Arfin, M. A. Long, M. S. Fee, and R. Sarpeshkar, "Wireless neural stimulation in freely behaving small animals," *Journal of Neurophysiology*, vol. 102, no. 1, pp. 598–605, Apr. 2009.

[4] H. M. Lee and M. Ghovanloo, "A high frequency active voltage doubler in standard CMOS using offset-controlled comparators for inductive power transmission," *in press IEEE Transactions on Biomedical Circuits and Systems*, vol. PP, no. 99, pp. 1–12, 2013.

[5] E. Noorsal, K. Sooksood, X. Hongcheng, R. Hornig, J. Becker, and M. Ortmanns, "A neural stimulator frontend with high-voltage compliance and programmable pulse shape for epiretinal implants," *IEEE Journal of Solid-State Circuits*, vol. 47, no. 1, pp. 244–256, Jan. 2012.

[6] L. Wu, Z. Yang, E. Basham, and W. Liu, "An efficient wireless power link for high voltage retinal implant," in *Proceedings of the IEEE Biomedical Circuits and Systems Conference*, Nov. 2008, pp. 101–104.

[7] F. Mounaim and M. Sawan, "Integrated high-voltage inductive power and data-recovery front end dedicated to implantable devices," *IEEE Transactions on Biomedical Circuits and Systems*, vol. 5, no. 3, pp. 283–291, Jun. 2011.

[8] *REF200, Dual current source/current sink*, PDS-851D, Texas Instruments, Oct. 1993.

[9] S. Nag, X. Jia, N. V. Thakor, and D. Sharma, "Flexible charge balanced stimulator with 5.6 fC accuracy for 140 nC injections," *in press, IEEE Transactions on Biomedical Circuits and Systems*, no. 99.